



Article

# N-Type Bismuth Telluride Nanocomposite Materials Optimization for Thermoelectric Generators in Wearable Applications

Amin Nozariasbmarz <sup>1,2</sup>, Jerzy S. Krasinski <sup>3</sup> and Daryoosh Vashaee <sup>1,2,\*</sup>

- Department of Electrical and Computer Engineering, Monteith Research Center, North Carolina State University, Raleigh, NC 27606, USA; anozari@ncsu.edu
- Department of Materials Science and Engineering, North Carolina State University, Raleigh, NC 27695, USA
- School of Electrical and Computer Engineering, Helmerich Advanced Technology Research Center, Oklahoma State University, Tulsa, OK 74106, USA; krasins@okstate.edu
- \* Correspondence: dvashae@ncsu.edu; Tel.: +1-(919)-515-9599

Received: 29 March 2019; Accepted: 2 May 2019; Published: 10 May 2019



**Abstract:** Thermoelectric materials could play a crucial role in the future of wearable electronic devices. They can continuously generate electricity from body heat. For efficient operation in wearable systems, in addition to a high thermoelectric figure of merit, zT, the thermoelectric material must have low thermal conductivity and a high Seebeck coefficient. In this study, we successfully synthesized high-performance nanocomposites of n-type  $Bi_2Te_{2.7}Se_{0.3}$ , optimized especially for body heat harvesting and power generation applications. Different techniques such as dopant optimization, glass inclusion, microwave radiation in a single mode microwave cavity, and sintering conditions were used to optimize the temperature-dependent thermoelectric properties of  $Bi_2Te_{2.7}Se_{0.3}$ . The effects of these techniques were studied and compared with each other. A room temperature thermal conductivity as low as 0.65 W/mK and high Seebeck coefficient of  $-297 \text{ }\mu\text{V/K}$  were obtained for a wearable application, while maintaining a high thermoelectric figure of merit, zT, of 0.87 and an average zT of 0.82 over the entire temperature range of  $25 \,^{\circ}\text{C}$  to  $225 \,^{\circ}\text{C}$ , which makes the material appropriate for a variety of power generation applications.

**Keywords:** n-type bismuth telluride; thermoelectric materials; nanocomposites; wearable systems; body heat harvesting; power generation

## 1. Introduction

One of the most promising technologies for waste heat recovery from environmental sources is based on thermoelectric generators in which the temperature gradient is directly converted to electricity. The conversion efficiency of the thermoelectric materials depends on the thermoelectric dimensionless figure of merit, zT, i.e.:

$$zT = \frac{S^2 \sigma}{\kappa} T \tag{1}$$

where S is the Seebeck coefficient in  $\mu V/K$ ,  $\sigma$  is the electrical conductivity in S/cm,  $\kappa$  is the thermal conductivity (including lattice component  $\kappa_L$ , electronic component  $\kappa_e$ , and bipolar component  $\kappa_{bi}$ ) in W/mK, and T is the absolute temperature in K [1]. Improving zT has always been challenging because S,  $\sigma$ , and  $\kappa$  are interdependent.

Materials **2019**, 12, 1529 2 of 13

The electrical conductivity is defined by  $\sigma = ne\mu$ , where n, e, and  $\mu$  are the charge carrier concentration, charge (=1.6 × 10<sup>-19</sup> coulombs) and mobility, respectively [2]. By adding this to Equation (1) and rearranging, we can write:

$$zT = (S^2 n) \left(\frac{\mu}{\kappa}\right) eT \tag{2}$$

The components in the two parentheses are counter-indicated [3]. According to the Pisarenko relation [4], higher n results in lower S, while defects reduce both  $\kappa$  and  $\mu$ . Therefore, there is always a trade-off among these properties.

While the initial application of thermoelectric materials for power generation was in spacecraft such as Voyager, Cassini, and New Horizons [5], they have recently been used in other applications, such as in vehicles for waste heat recovery, and power generation from body heat in self-powered wearable health sensors [6–9]. Traditionally, studies have been focused primarily on improving only zT of the thermoelectric materials [6,10–16]. Thus, high zT values have been achieved for a variety of materials [17–21]. However, as we will discuss, the individual material properties, namely  $\kappa$  and S, can play key roles even more than zT when the material is used in wearable systems.

A thermoelectric generator (TEG) produces electricity by recovering energy from the (waste) heat of environmental sources. This unique capability makes TEGs a favorable method for energy harvesting from the body. Thermal energy is a continuous energy source from the body, in contrast to mechanical input applied by the user, sunlight, or ambient radio waves, which can be interrupted at times. A self-powered wearable device requires control of the performance of thermoelectric materials and device together [22]. For body wearable TEGs, the performance is limited by the hot side (skin) and cold side (ambient) heat exchangers due to large parasitic thermal resistances [23]. In addition to a high zT, the material must have low thermal conductivity. This requirement is mainly due to the skin thermal resistance and the constraints limiting the use of a heat sink in a wearable platform. A larger output voltage at the device level is also required to run the boost converter and the power management unit efficiently. This is fulfilled through materials with high Seebeck coefficients. Therefore, these conditions require the TEG to be designed not only with specific consideration of leg geometries and spacing, but also careful consideration of material properties.

Bismuth telluride ( $Bi_2Te_3$ ) alloys have been developed since the 1960s, and are the most promising thermoelectric materials for low-temperature applications [24]. N-type  $Bi_2Te_3$  alloys theoretically suffer from low zT due to the restricted number of valleys near the conduction band edge. Recently, researchers have reported zT improvements in n-type  $Bi_2Te_3$  alloys using zone melting [25], nanostructuring [26–28], nano-inclusions [29], texturing [30], and point defect engineering [31]. Although there are a few studies that have shown high zT values for n-type  $Bi_2Te_3$ , these materials are not appropriate for applications such as body heat harvesting due to their non-optimized properties at body temperature. Therefore, optimizing the transport properties of n-type  $Bi_2Te_3$  alloys around body (or room) temperature is highly desired.

For body heat harvesting applications, thermoelectric materials require a combination of high zT, low  $\kappa$ , and high S at room temperature [23]. For applications at above 100 °C (i.e., power generation), low  $\kappa$  is not determinative; however, high S and zT are still demanded. To fulfill these requirements, we synthesized optimized nanostructured n-type materials based on Bi<sub>2</sub>Te<sub>2.7</sub>Se<sub>0.3</sub>. We investigated the effect of several parameters, including dopant addition, tellurium vacancies, glass inclusion, sintering time and temperature, microwave processing, and subsequent annealing, primarily to fully optimize the thermoelectric properties of bulk nanostructured n-type Bi<sub>2</sub>Te<sub>2.7</sub>Se<sub>0.3</sub> materials. N-type materials with a thermal conductivity as low as 0.65 W/mK, Seebeck coefficients as high as  $-297~\mu$ V/K, peak zT of 0.87, and average zT of 0.82 were achieved. The results show that different parameters can shift maximum zT from room temperature to above 100 °C. Materials with excellent properties at room temperature are desired for wearable applications, while those with good features at above 150 °C are useful for high-temperature power generation.

Materials **2019**, 12, 1529 3 of 13

#### 2. Experimental Section

Stoichiometric ratios of high purity elements of Bi powder (99.9% purity), Te lump (99.9% purity), and Se powder (99.9% purity) were milled for two hours in a planetary ball mill (Fritsch-P7) using a tungsten carbide bowel and zirconia balls under 950 rpm speed and ball-to-powder ratio of 5:1 to prepare uniform nano-sized  $\rm Bi_2Te_{3-x}Se_x$  powders. The milling process of all samples was similar.

Additionally, the stoichiometric ratio of high purity elements of Bi powder and Te lump were milled for 15 min in similar conditions and melted in an induction furnace (IF) to prepare homogenized  $Bi_2Te_3$  ingots. The process was fulfilled in a graphite die inside a quartz tube under argon atmosphere. The ingots were crushed and milled for 5 h in a planetary ball mill (Fritsch-P6) using a tungsten carbide bowel and balls under 500 rpm and a ball-to-powder ratio of 10:1 to prepare a uniform nano-sized  $Bi_2Te_3$  powders. Se of 6 atomic percent (at. %) was subsequently added to the  $Bi_2Te_3$  powder and milled for one hour to obtain a uniform powder. To tune the thermal conductivity and Seebeck coefficient, 2.5 at. % glass (Ferro-EG 2964) powder was added to the mixture. The names, compositions, synthesis parameters, room temperature Seebeck coefficient, thermal conductivity, zT, and maximum zT of the synthesized materials are further listed in Table 1.

<b>Table 1.</b> List of names, compositions, synthesis parameters, room temperature Seebeck coefficients,
thermal conductivities, $zT$ , and maximum $zT$ of the synthesized materials.

Name	Material	1st SPS T (°C)/Soak Time (min) *	MW Process	2nd SPS T (°C)/Soak Time (min)	Room T S (μV/K)	Room T κ (W/mK)	Room T	Max zT
S1	Bi <sub>2</sub> Te <sub>3</sub>	540/1	Yes	450/1	-132	1.95	0.37	0.57
S2	Bi <sub>2</sub> Te <sub>3</sub> -0.3%Se **	540/1	Yes	450/1	-163	1.28	0.70	0.89
S3	Bi <sub>2</sub> Te <sub>2.7</sub> Se <sub>0.3</sub>	540/2	No	-	-266	0.78	0.72	0.72
S4	Bi <sub>2.04</sub> Te <sub>2.66</sub> Se <sub>0.3</sub>	540/2	No	-	-120	0.79	0.15	0.24
S5	Bi <sub>2.15</sub> Te <sub>2.55</sub> Se <sub>0.3</sub>	540/2	No	-	-58	1.57	0.11	0.33
S6	Bi <sub>2</sub> Te <sub>2.7</sub> Se <sub>0.3</sub> -2.5%Glass	540/1	No	-	-256	0.78	0.72	0.72
S7	Bi <sub>2</sub> Te <sub>2.7</sub> Se <sub>0.3</sub> -2.5%Glass	540/2	No	-	-268	0.70	0.57	0.57
S8	Bi <sub>2</sub> Te <sub>2.7</sub> Se <sub>0.3</sub> -2.5%Glass	540/3	No	-	-283	0.73	0.39	0.39
S9	Bi <sub>2</sub> Te <sub>2.7</sub> Se <sub>0.3</sub> -2.5%Glass	540/2	Yes	450/1	-284	0.77	0.59	0.59
S10	Bi <sub>2</sub> Te <sub>2.7</sub> Se <sub>0.3</sub> -2.5%Glass	540/3	Yes	450/1	-297	0.65	0.63	0.63
S11	Bi <sub>2</sub> Te <sub>2.7</sub> Se <sub>0.3</sub> -2.5%Glass	310/1	Yes	450/1	-188	0.78	0.67	0.87
S12	Bi <sub>2</sub> Te <sub>2.7</sub> Se <sub>0.3</sub> -2.5%Glass	270/1	Yes	450/1	-204	0.91	0.63	0.70
S13	Bi <sub>2</sub> Te <sub>3</sub> -0.3%Se	310/1	Yes	450/1	-121	1.34	0.46	0.77
S14	$\mathrm{Bi_{2}Te_{2.7}Se_{0.3}}$	540/2	Yes	450/1	-263	0.79	0.76	0.76
S15-a300-24	Bi <sub>2</sub> Te <sub>2.7</sub> Se <sub>0.3</sub> (anneal at 300°C/24h)	540/2	Yes	450/1	-283	0.85	0.68	0.68

<sup>\*</sup> Table abbreviations: SPS: spark plasma sintering, T: temperature, MW: microwave. \*\* 0.3% Se is equal to 6 at. % Se.

The synthesized powders were sintered in a cylindrical graphite die with an inner diameter of 6 mm at different temperatures using spark plasma sintering (SPS), to make the thermoelectric ingots with 6 mm diameter and 14 mm height. The temperature was monitored using a k-type thermocouple placed at the center of the die, close to the center of the sample.

The effect of microwave (MW) processing was studied using a rectangular single mode cavity attached to a 2.45 GHz (1 kW) generator. The experimental set up is shown in Figure 1. It contains a magnetron as the source that provides a stable and tunable MW energy [32]. A waveguide was used to direct the electromagnetic wave and restrict the field. An electric and magnetic field (E-H) tuner and a sliding short was used for convenient tuning and load matching during the exposure of the specimen [33,34]. The sample was placed in the center of the waveguide where the electric field is maximum. The material was heated up volumetrically by MW absorption, leading to rapid sintering [35,36].

Materials **2019**, 12, 1529 4 of 13

The electrical resistivity and Seebeck coefficients of the samples were simultaneously measured using the commercially available Ulvac instrument, ZEM-3, from room temperature to 250 °C. The thermal diffusivity (D) was measured by a laser flash instrument (Netzsch's LFA 457 Micro Flash) from room temperature to 250 °C. The specific heat capacity ( $C_p$ ) was calculated for Bi<sub>2</sub>Se<sub>0.3</sub>Te<sub>2.7</sub> alloy according to the theoretical data. The thermal conductivity of the samples was derived from the relationship  $\kappa = \rho DC_p$ , where  $\rho$  is the mass density of the samples measured using Archimedes' principle.

SPS and MW are used in this paper as the abbreviation for spark plasma sintering and microwave, respectively.

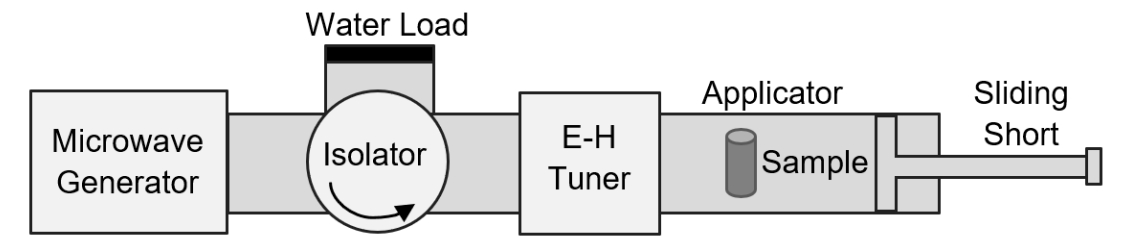


**Figure 1.** Schematic view of the microwave (MW) set-up. The sample is placed at the center of the waveguide where the electric field is maximum.

#### 3. Results and Discussion

### 3.1. Effect of Dopant Addition

In  $Bi_2Te_3$  alloy, excess Bi and Te atoms lead to p- and n-type semiconducting behavior, respectively. These excess atoms make anti-site defects by penetrating into the lattice structure [37]. In fact, the doping mechanism in a pure  $Bi_2Te_3$  alloy is mainly through anti-site and vacancy defects. The  $Bi_{Te}$  anti-site donates one hole, and the  $Te_{Bi}$  anti-site provides one electron. Furthermore, Bi vacancy donates 3 holes, and Te vacancy provides 2 electrons [38–41]. The formation energy of  $Te_{Bi}$  anti-site defect is lower than the Te vacancy and  $Bi_{Te}$  anti-site, hence, it is the most abundant doping mechanism in  $Bi_2Te_3$  alloy [40]. Formation of Te vacancies in Te0 resulting in the presence of the Te1 remineration band that reduces the power factor (Te2 resulting in the presence to Te3 can tune the anion vacancies, which results in power factor enhancement [31].

Figure 2 shows electrical conductivity, Seebeck coefficient, power factor times temperature (PFT), thermal conductivity, and zT of S1 and S2 as a function of temperature in the range of 25 °C to 225 °C. The Seebeck coefficient and high electrical conductivity of S1 reveals that it has an excessively high carrier concentration. The negative sign of the Seebeck coefficient is due to the n-type characteristic of Bi<sub>2</sub>Te<sub>3</sub>. Addition of Se dopant to S1 tuned the carrier concentration and improved the power factor up to 13%, and decreased the thermal conductivity by 30%. This resulted in a zT of 0.67 at room temperature in S2, which is 60% higher than that of S1. S2 also showed an average zT of 0.82 in the temperature range of 25 to 225 °C. The bipolar effect in this alloy occurs at ~150 °C, and addition of selenium dopant does not shift the bipolar effect to a lower temperature.

Materials **2019**, 12, 1529 5 of 13

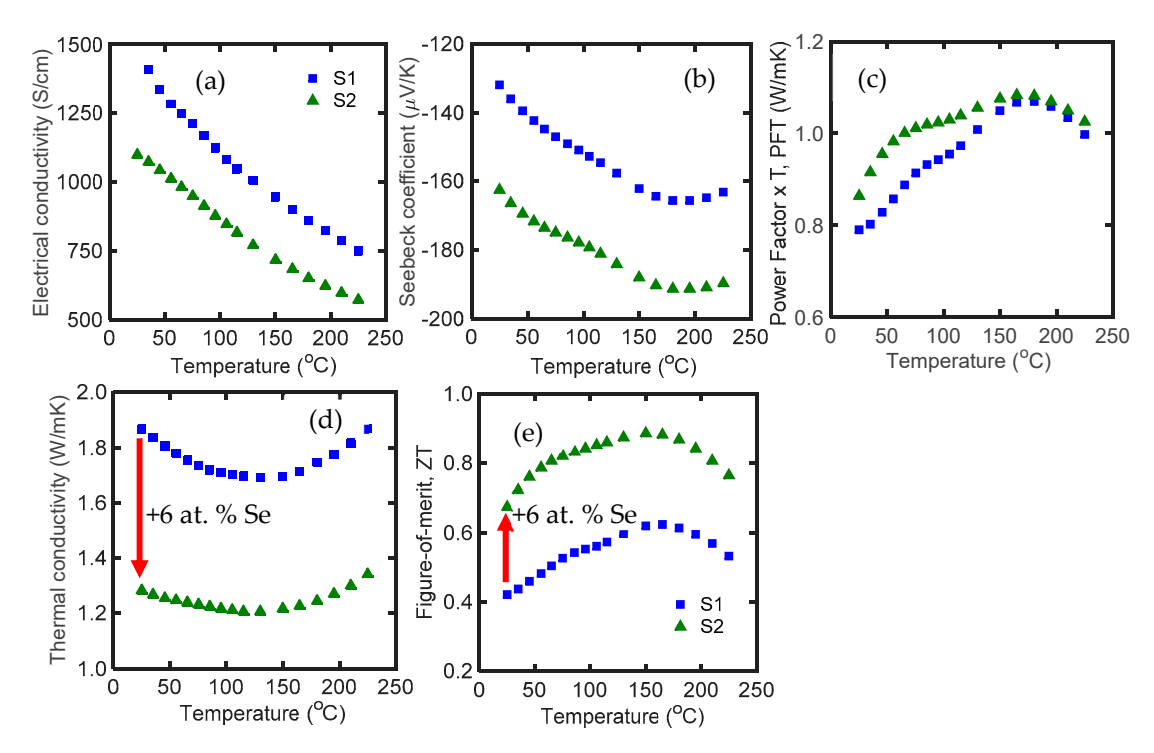


**Figure 2.** (a) Electrical conductivity; (b) Seebeck coefficient; (c) power factor  $\times$  temperature; (d) thermal conductivity; and (e) zT of S1 and S2 as a function of temperature in the range of 25 °C to 225 °C. According to Table 1, S1 is a pure Bi<sub>2</sub>Te<sub>3</sub>, and S2 is Bi<sub>2</sub>Te<sub>3</sub> with 6 at. % Se.

## 3.2. Optimizing Te Vacancy

Te vacancy can control the thermoelectric properties of n-type  $Bi_2Te_3$  alloys by adjusting the Fermi level and transport properties. According to Figure 3, the reduction of Te content from the stoichiometric ratio (i.e., S4 and S5) led to a dramatic drop in thermoelectric properties. Te vacancies result in highly doped n-type materials. According to the extremely high electrical conductivity and low value of the Seebeck coefficient, S5 is a highly doped material with electrical conductivity six times higher than S3 at room temperature (Figure 3a,b). The electrical conductivity of S4 was identical to S3 in all the temperature ranges (Figure 3a). The low electrical conductivity of S4 is due to the small carrier mobility. S3 had the highest PFT below 150 °C (Figure 3c). Smaller PFT in S4 and S5 is due to the Te vacancies, which move the Fermi level deep in the conduction band [28]. The thermal conductivity of S3 and S4 was similar up to 100 °C, then it differentiated at higher temperatures (Figure 3d). Non-optimized thermoelectric properties of S4 and S5 resulted in very low zT in these samples. According to this result, for 6 at. % Se,  $Bi_{2.0}Te_{2.7}Se_{0.3}$  has the optimum Te vacancy concentration. Selenium dopant effectively compensated Te vacancies in S3, and it had a maximum zT of 0.72 at room temperature. Further zT improvement of S4 and S5 requires optimization of the amount of Se in this alloy.

Materials **2019**, 12, 1529 6 of 13

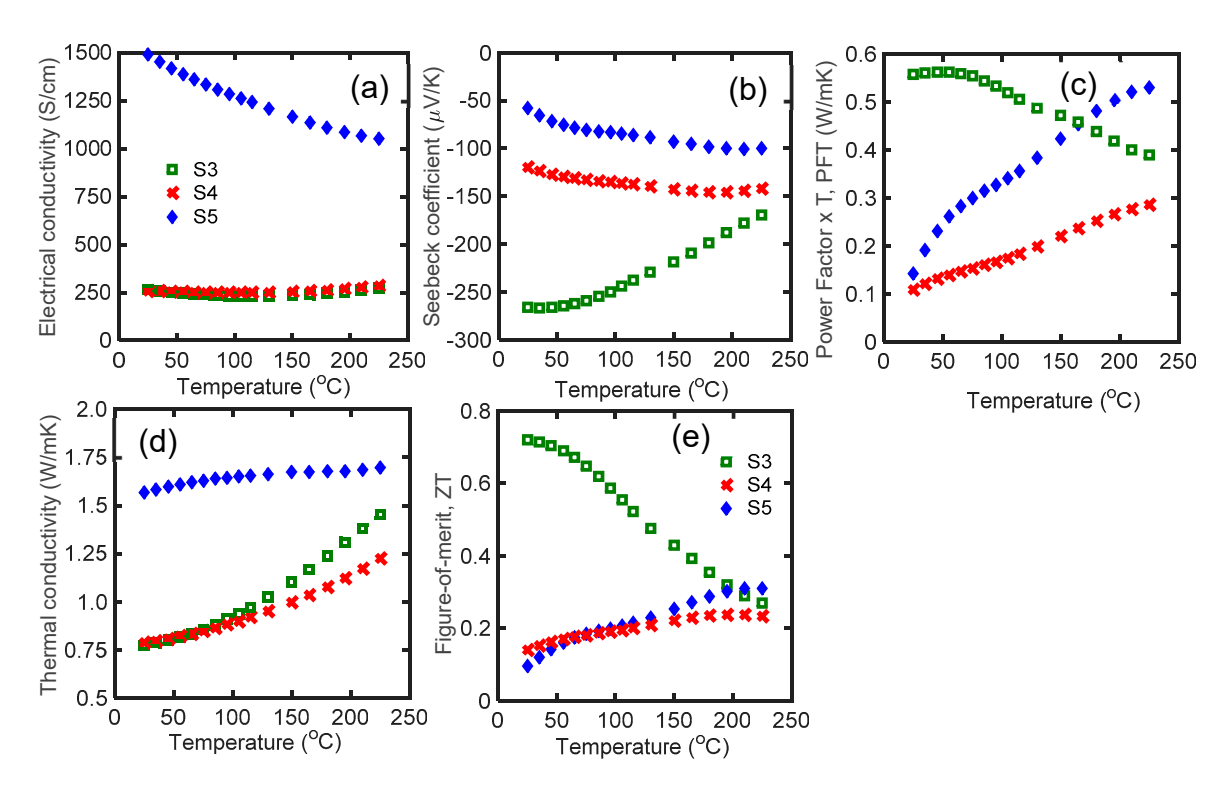


**Figure 3.** (a) Electrical conductivity; (b) Seebeck coefficient; (c) power factor  $\times$  temperature; (d) thermal conductivity; and (e) zT of S3, S4, and S5 samples as a function of temperature in the range of 25 °C to 225 °C. The compositions of S3, S4, and S5 are  $Bi_{2.00}Te_{2.70}Se_{0.3}$ ,  $Bi_{2.04}Te_{2.66}Se_{0.3}$ , and  $Bi_{2.15}Te_{2.55}Se_{0.3}$ , respectively.

#### 3.3. Effect of Glass Inclusion and Soaking Time

Figure 4 shows the thermoelectric properties of S6, S7, and S8 as a function of temperature in the range of 25  $^{\circ}$ C to 225  $^{\circ}$ C. The effects of addition of 2.5 at. % glass inclusion into Bi<sub>2.0</sub>Te<sub>2.7</sub>Se<sub>0.3</sub> along with 1, 2, and 3 min soaking times were studied. All samples were sintered at 540  $^{\circ}$ C.

The electrical conductivity of the samples reduced with increased soaking time (Figure 4a). S8 had the highest electrical conductivity at room temperature, equal to 287 S/cm, and S10 had the lowest, equal to 121 S/cm. The electrical conductivity of the samples with glass inclusions dropped with soaking time. The variation of electrical conductivity among the samples become small at higher temperatures (>150  $^{\circ}$ C) due to the dominance of the acoustic phonon scattering mechanism.

Glass inclusion improved the Seebeck coefficient of the samples, and the soaking time had an extra constructive effect on increasing the Seebeck coefficient at room temperature. S8 had the highest Seebeck coefficient, equal to  $-283~\mu\text{V/K}$ . The absolute value of the Seebeck coefficient decreased with temperature over the entire temperature range. Over 75 °C, S6 showed the maximum Seebeck coefficient. The glass nano-inclusions provide new barriers for the charge carriers (i.e., electrons). High energy electrons can overcome the barrier energy and pass through the barrier; however, low energy electrons are reflected. This technique increases the mean energy of the electrons with respect to the Fermi energy, and thus increases the overall Seebeck coefficient.

The PFT of all samples decreased with temperature, and the soaking time impaired the PFT of the nanocomposites. S6 had the maximum PFT of 0.56 W/mK at room temperature. Thermal conductivity was monotonically enhanced with temperature in all glass-included samples. S6 had the highest room temperature thermal conductivity, equal to  $\sim 0.78$  W/mK, and higher soaking times resulted in a reduction of the thermal conductivity up to 10% (Figure 4d).

All zTs were maximum near room temperature. The maximum zT values of the S6, S7, and S8 samples were 0.72, 0.57 and 0.39, respectively (Figure 4e). The sample with 1 min soaking time had the highest zT throughout the temperature range. Although longer soaking time led to an improved

Materials **2019**, 12, 1529 7 of 13

Seebeck coefficient and reduced the thermal conductivity by ~10%, it had a dramatic destructive effect on zT of n-type nanocomposites of Bi<sub>2.0</sub>Te<sub>2.7</sub>Se<sub>0.3</sub>-2.5% glass samples by up to 46%. Therefore, for specimens with glass inclusions, shorter soaking time is required.

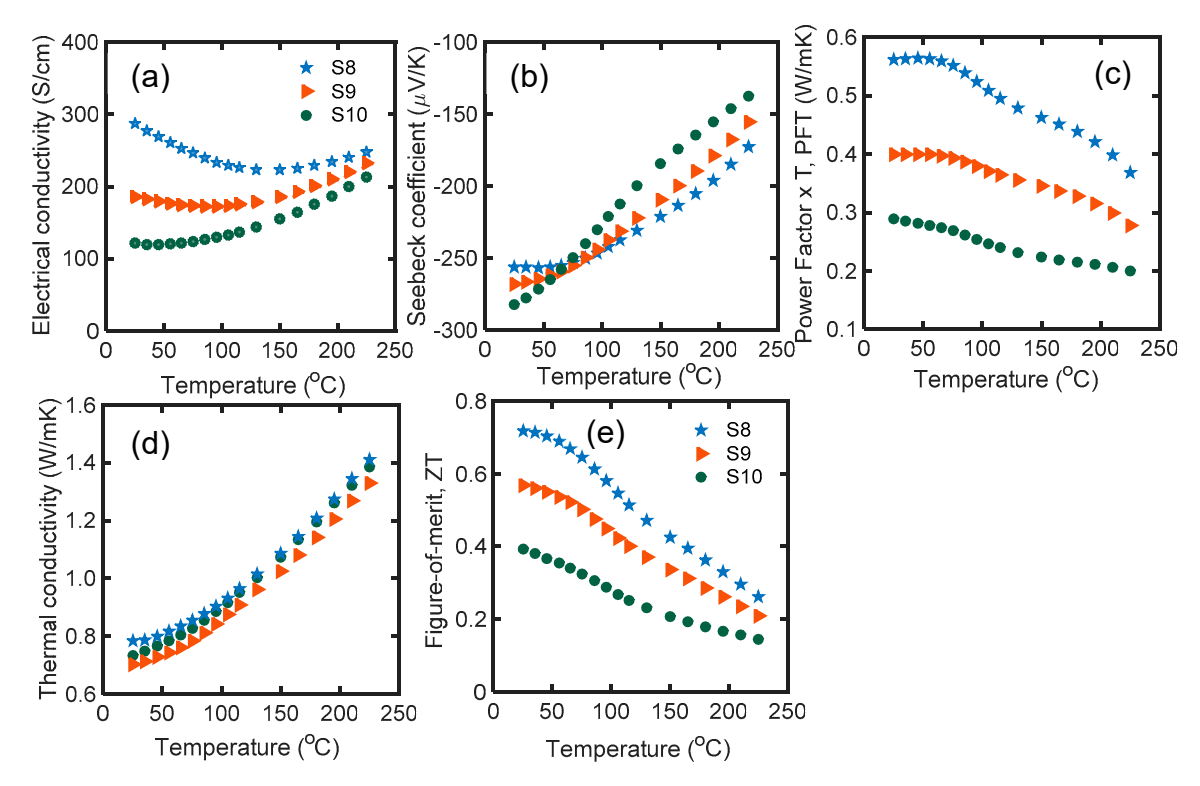


**Figure 4.** (a) Electrical conductivity; (b) Seebeck coefficient; (c) power factor times temperature (PFT); (d) thermal conductivity, and (e) zT of S6, S7, and S8 samples as a function of temperature in the range of 25 °C to 225 °C. A 2.5 at. % glass inclusion was added to Bi<sub>2.0</sub>Te<sub>2.7</sub>Se<sub>0.3</sub>. S6, S7, and S8 were sintered at 540 °C with 1, 2 and 3 min soaking time, respectively.

#### 3.4. Effect of Microwave Processing with Glass Inclusion

Figure 5 depicts the thermoelectric properties of S7, S8, S9, and S10 samples as a function of temperature in the range of 25  $^{\circ}$ C to 225  $^{\circ}$ C. S9 and S10 are S7 and S8 after microwave processing, respectively. As mentioned, S7 and S8 are samples with 2.5 at. % glass inclusions, sintered at 540  $^{\circ}$ C for 2 and 3 min, respectively.

The room temperature electrical conductivity of S7 did not change after microwave radiation (S9), while the room temperature electrical conductivity of S8 was improved by 30% after microwave processing (S10). At higher temperatures, microwave processing resulted in an electrical conductivity drop in S9, while it did not affect S10 (Figure 5a).

The absolute value of the Seebeck coefficients of S9 and S10 improved by 6% and 5%, respectively. S10 had the maximum Seebeck coefficient, equal to  $-297~\mu\text{V/K}$  (Figure 5b), which is one of the highest reported values in the literature. The PFT of S7 and S8 increased by 13.7% (S9) and 42% (S10) respectively after microwave processing (Figure 5c). The improved thermoelectric PFT of the microwave processed samples in comparison to SPS samples is also due to the non-linear transport of charge carriers between the decrystallized grains with compositional variation and/or disordered-crystalline regions [42–44].

Glass inclusion generally reduces the thermal conductivity of  $Bi_{2.0}Te_{2.7}Se_{0.3}$ . The thermal conductivity of all glass-included samples increased monotonically with temperature. According to Figure 5d, the thermal conductivity of S9 (S7 after microwave processing) was increased by 10%. In contrast, the thermal conductivity of S10 (S8 after microwave processing) dropped by 12%. Because S8 initially had poor thermoelectric properties, it is probable that glass inclusion played a constructive role in reducing the thermal conductivity of S10.

Materials **2019**, 12, 1529 8 of 13

The microwave processed samples (S9 and S10) had higher zT values compared to their initial SPS samples (S7 and S8). The zT of all samples decreased with temperature over the entire temperature range. Figure 5e shows that S10 had the highest zT, equal to 0.63. At room temperature, zT of S8 increased by 60% after microwave processing, and zT of S9 slightly improved after microwave processing. In general, microwave processing enhanced the electrical conductivity, Seebeck coefficient, and zT of the glass-included samples, which shows that microwave processing is a reliable technique with which to engineer the thermoelectric properties of materials.

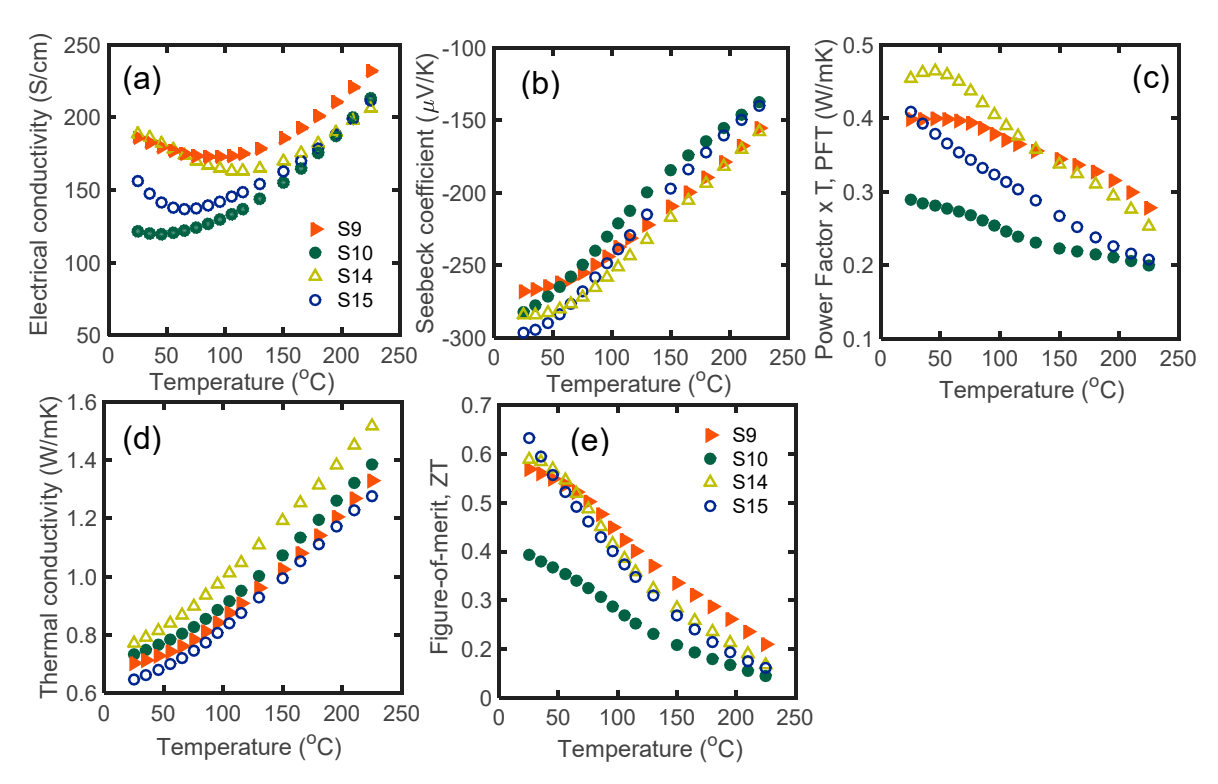


**Figure 5.** (a) Electrical conductivity; (b) Seebeck coefficient; (c) PFT; (d) thermal conductivity; and (e) *zT* of S7, S8, S9, and S10 as a function of temperature in the range of 25 °C to 225 °C. According to Table 1, S9 and S10 are the microwave processed forms of S7 and S8, respectively.

# 3.5. Effect of Initial SPS Temperature

Figure 6 shows (a) electrical conductivity, (b) Seebeck coefficient, (c) PFT, (d) thermal conductivity, and (e) zT of S6, S11, S12, S2, and S13 as a function of temperature in the range of 25 °C to 225 °C. S6 and S2 are depicted in this figure for comparison with other samples.

S6, S11, and S12 contained glass inclusions. Comparison of the electrical conductivity of these samples revealed that initial SPS at  $310~^{\circ}$ C, along with microwave processing, resulted in larger electrical conductivity (Figure 6a). The electrical conductivity of S11 decreased from S11 S/cm at room temperature to S11 S/cm at S11 C. Similarly, for S11 TeS11 Se samples (S11), lower initial hot press temperature resulted in higher electrical conductivity throughout the temperature range. The electrical conductivity of S11 amonotonically decreased with temperature. It seems that the carrier concentration in low-temperature SPS samples is higher than others.

S11, S12, S2, and S13 showed lower Seebeck coefficients compared to the previous samples (Figure 6b). Since the Seebeck coefficient is a strong function of the carrier concentration [45], a smaller absolute value of the Seebeck coefficient confirms the higher carrier concentration in all low-temperature SPS samples.

S6, S11, and S12 (all with glass inclusion) had almost similar PFT values,  $\sim$ 0.55 W/mK at room temperature (Figure 6c). The PFT of S11 and S12 increased up to 170 °C, then decreased. S2 and S13

Materials **2019**, 12, 1529 9 of 13

(samples without glass inclusion) had higher PFT values throughout the temperature range. S2 had 20% higher PFT than S13, and its PFT was >1 W/mK over 65 °C.

S11 had similar thermal conductivity to S6 at room temperature, and its thermal conductivity increased by a lower slope at a higher temperature. The variation of thermal conductivity versus temperature for samples with lower initial SPS temperature (i.e., 310 and 270 °C) was less than the samples which were initially sintered at 540 °C. The thermal conductivity of S12 was higher than S11 throughout the temperature range. S2 and S13 had greater room temperature thermal conductivity. It can be concluded that nanocomposite samples with glass inclusions, sintered at either low or high temperature, generally show lower thermal conductivity compared to the nanostructured samples sintered with similar conditions.

S6 had the highest zT at room temperature (Figure 6e). For glass included samples, S11 had a higher zT over 35 °C, and it had an average zT of 0.81 from 25 °C to 225 °C. Among the S6, S11, S12, S2, and S13 samples, S6 had the best properties for wearable application due to its having the highest Seebeck coefficient, lowest thermal conductivity, and highest zT at room temperature. Additionally, samples S2 and S11 had zT > 0.8 in the broad range of 50–175 °C. These samples are appropriate candidates for power generation applications. For the glass containing samples, initial SPS at lower temperature led to higher electrical conductivity, lower Seebeck coefficient, and similar thermal conductivity over the whole temperature range.

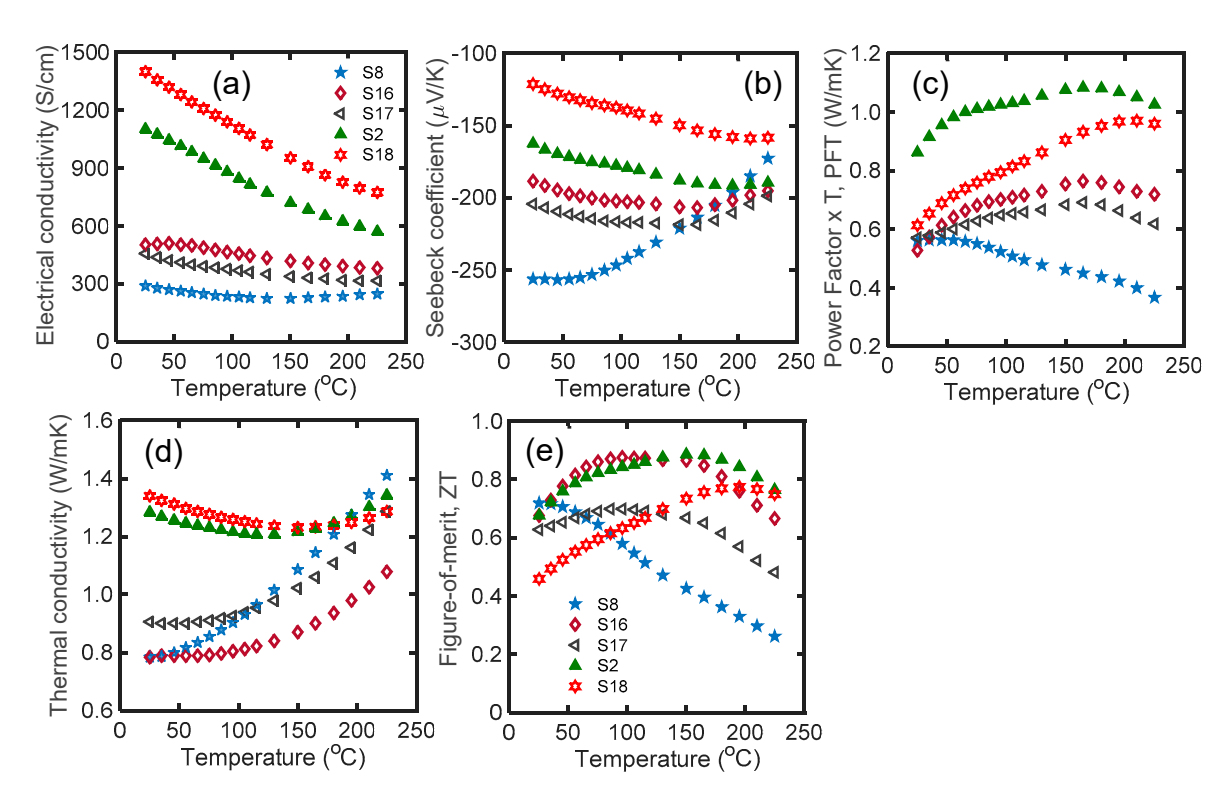


**Figure 6.** (a) Electrical conductivity; (b) Seebeck coefficient; (c) PFT; (d) thermal conductivity; and (e) zT of S6, S11, S12, S2, and S13 samples as a function of temperature in the range of 25 °C to 225 °C. According to Table 1, the composition and processing of the samples are as follows: S6: Bi<sub>2.0</sub>Te<sub>2.7</sub>Se<sub>0.3</sub>-2.5% glass, SPS at 540 °C for 1 min; S11: Bi<sub>2.0</sub>Te<sub>2.7</sub>Se<sub>0.3</sub>-2.5% glass, SPS at 310 °C for 1 min, microwave processed and post SPS at 450 °C; S12: Bi<sub>2.0</sub>Te<sub>2.7</sub>Se<sub>0.3</sub>-2.5% glass, SPS at 270 °C for 1 min, microwave processed and post SPS at 450 °C; S2: Bi<sub>2</sub>Te<sub>3</sub>-6 at. % Se, SPS at 540 °C for 1 min, microwave processed and post SPS at 450 °C; and S13: Bi<sub>2</sub>Te<sub>3</sub>-6 at. % Se, SPS at 310 °C for 1 min, microwave processed and SPS at 450 °C.

### 3.6. Effect of Annealing

Figure 7 shows the thermoelectric properties of S14 and S14-a300-24 as a function of temperature in the range of 25 °C to 225 °C. The processing conditions are explained in Table 1. The electrical conductivity of S14 decreased throughout the temperature range after 24 h annealing at 300 °C. The room temperature electrical conductivity dropped by 18.5%, while the absolute value of the Seebeck coefficient increased by 8% after annealing. The carrier concentration has dropped probably due to the annealing of the anti-site and vacancies. The PFT of the annealed sample fell over the entire temperature range. The thermal conductivity of the annealed sample increased due to the grain growth at 300 °C. Increased grain size results in lower interaction of phonons with grain boundaries that can improve the  $\kappa_L$ . The zT values of both samples monotonically decreased by temperature. The room temperature zT of S14 dropped by ~12% after annealing. The variation between the zT of S14 and S14-a300-24 was almost constant over the temperature range. It is concluded that, although annealing at 300 °C resulted in higher Seebeck coefficient at room temperature, it increased the thermal conductivity and reduced the zT.

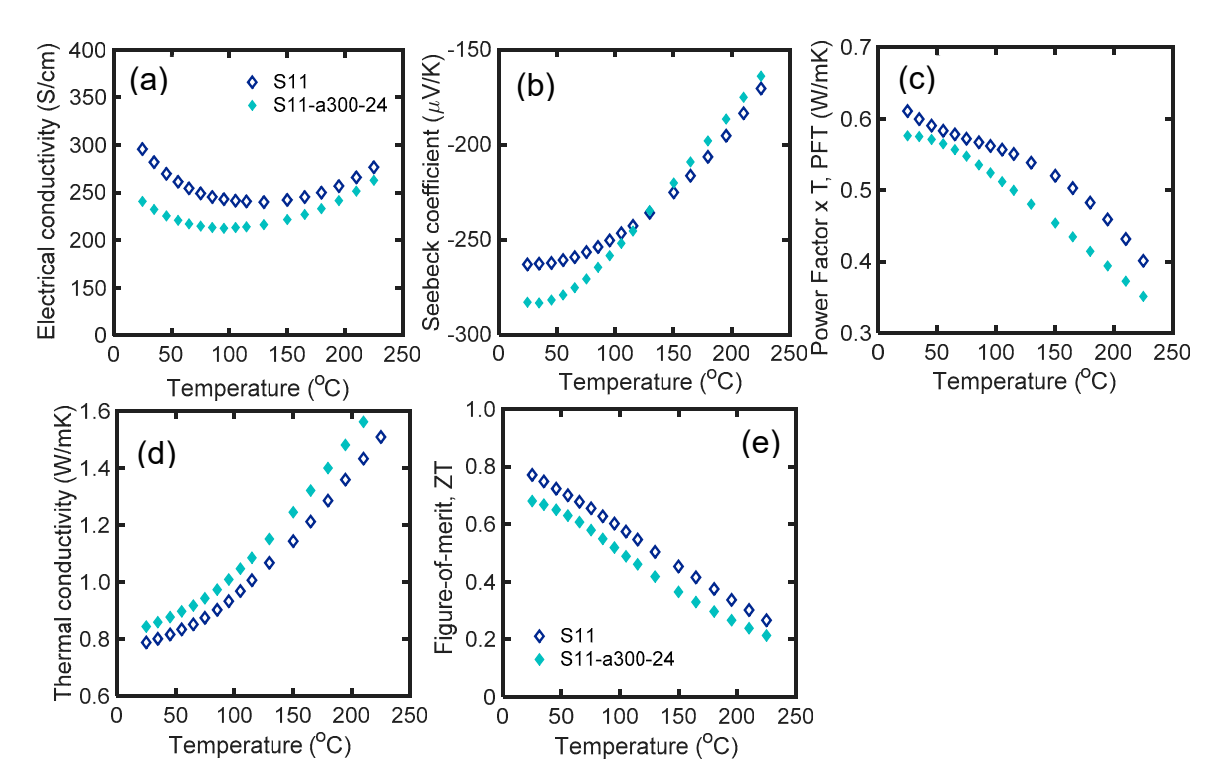


**Figure 7.** (a) Electrical conductivity; (b) Seebeck coefficient; (c) PFT; (d) thermal conductivity; and (e) zT of S14 and S14-a300-24 samples as a function of temperature in the range of 25 °C to 225 °C. According to Table 1, S14-a300-24 is S14 after annealing at 300 °C for 24 h.

## 4. Conclusions

We synthesized high-performance nanocomposites of n-type  $Bi_2Te_{2.7}Se_{0.3}$  for body heat harvesting and power generation applications. The effects of several parameters, including dopant addition, tellurium vacancy, glass inclusion, microwave processing, SPS soaking time and temperature, and subsequent annealing were studied to optimize the thermoelectric properties of the synthesized materials. In general, the addition of a Se dopant resulted in both power factor enhancement and thermal conductivity reduction. Tellurium vacancy can drop the power factor of n-type  $Bi_2Te_3$  alloys significantly. An optimum amount of selenium dopant is required to compensate for the loss. Glass inclusion reduced the thermal conductivity and improved the Seebeck coefficient of the alloys. However, a longer soaking time decreased the zT of the glass-included samples. Microwave processing enhanced

the electrical conductivity, Seebeck coefficient, and zT of the glass-included samples. It proved to be a reliable method to improve the thermoelectric properties of different materials. Annealing at 300 °C increased the thermal conductivity and reduced the zT, while it increased the Seebeck coefficient.

A room temperature thermal conductivity of 0.65 W/mK, Seebeck coefficient of  $-297~\mu\text{V/K}$  and zT = 0.76 were achieved which fulfill the combined requirements (low thermal conductivity, high Seebeck coefficient and high zT at room temperature) for body heat harvesting applications. The optimized materials in this study showed a peak zT of 0.87, and an average zT of 0.82 over the entire temperature range of 25–225 °C, and a high Seebeck coefficient, above  $-200~\mu\text{V/K}$ , which makes them suitable for a variety of power generation applications.

**Author Contributions:** A.N. and D.V. conceived the idea. A.N. performed the experiments. D.V. and J.S.K. supervised the research. All authors contributed to writing the paper and discussions.

**Funding:** This research was partially based upon work supported by Air Force Office of Scientific Research (AFOSR) under contract number FA9550-12-1-0225 and the National Science Foundation (NSF) under grant numbers EEC-1160483, ECCS-1351533, ECCS-1711253, and CMMI-1363485.

**Acknowledgments:** J.S.K. acknowledges the funding support from Oklahoma Center for the Advancement of Science & Technology (OCAST) Oklahoma Applied Research Support (OARS) program under Contract No. AR14-052.

Conflicts of Interest: The authors declare no conflict of interest.

#### References

- 1. Goldsmid, H.J. Introduction to Thermoelectricity; Springer: Heidelberg, Germany, 2009; Volume 121.
- Vining, C.B. Thermoelectric Properties of Silicides. In CRC Handbook of Thermoelectrics; CRC Press: Boca Raton, FL, USA, 1995; pp. 277–286.
- 3. Heremans, J.P.; Dresselhaus, M.S.; Bell, L.E.; Morelli, D.T. When thermoelectrics reached the nanoscale. *Nat. Nanotechnol.* **2013**, *8*, 471–473. [CrossRef]
- 4. Ioffe, A.F.; Stil'Bans, L.S.; Iordanishvili, E.K.; Stavitskaya, T.S.; Gelbtuch, A.; Vineyard, G. Semiconductor thermoelements and thermoelectric cooling. *Phys. Today* **1959**, *12*, 42. [CrossRef]
- 5. Schmidt, G.R.; Sutliff, T.J.; Dudzinksi, L.A. Radioisotope Power: A Key Technology for Deep Space Exploration. In *Radioisotopes—Applications in Physical Science*; Singh, N., Ed.; InTech: London, UK, 2011; p. 419.
- 6. Snyder, G.J.; Toberer, E.S. Complex thermoelectric materials. Nat. Mater. 2008, 7, 105–114. [CrossRef]
- 7. Bux, S.K.; Fleurial, J.P.; Kaner, R.B. Nanostructured materials for thermoelectric applications. *Chem. Commun.* **2010**, *46*, 8311–8324. [CrossRef] [PubMed]
- 8. Kishi, M.; Nemoto, H.; Hamao, T.; Yamamoto, M.; Sudou, S.; Mandai, M.; Yamamoto, S. Micro thermoelectric modules and their application to wristwatches as an energy source. In Proceedings of the 18th International Conference on Thermoelectrics, Baltimore, MD, USA, 29 August–2 September 1999; pp. 301–307.
- 9. Misra, V.; Bozkurt, A.; Calhoun, B.; Jackson, T.; Jur, J.S.; Lach, J.; Lee, B.; Muth, J.; Oralkan, Ö.; Öztürk, M.; Trolier-McKinstry, S.; et al. Flexible technologies for self-powered wearable health and environmental sensing. *Proc. IEEE* 2015, 103, 661–685. [CrossRef]
- 10. Minnich, A.J.L.; Dresselhaus, M.S.; Ren, Z.F.; Chen, G. Bulk nanostructured thermoelectric materials: Current research and future prospects. *Energy Environ. Sci.* **2009**, 2, 466–479. [CrossRef]
- 11. Dresselhaus, M.S.; Chen, G.; Tang, M.Y.; Yang, R.G.; Lee, H.; Wang, D.Z.; Ren, Z.F.; Fleurial, J.; Gogna, P. New Directions for Low-Dimensional Thermoelectric Materials. *Adv. Mater.* **2007**, *19*, 1043–1053. [CrossRef]
- 12. Zebarjadi, M.; Esfarjani, K.; Dresselhaus, M.S.; Ren, Z.F.; Chen, G. Perspectives on thermoelectrics: From fundamentals to device applications. *Energy Environ. Sci.* **2012**, *5*, 5147–5162. [CrossRef]
- 13. Vineis, C.J.; Shakouri, A.; Majumdar, A.; Kanatzidis, M.G. Nanostructured thermoelectrics: Big efficiency gains from small features. *Adv. Mater.* **2010**, *22*, 3970–3980. [CrossRef] [PubMed]
- 14. Biswas, K.; He, J.; Blum, I.D.; Wu, C.I.; Hogan, T.P.; Seidman, D.N.; Dravid, V.P.; Kanatzidis, M.G. High-performance bulk thermoelectrics with all-scale hierarchical architectures. *Nature* **2012**, *489*, 414–418. [CrossRef]
- 15. Sootsman, J.R.; Chung, D.Y.; Kanatzidis, M.G. New and old concepts in thermoelectric materials. *Angew. Chem. Int. Ed.* **2009**, *48*, 8616–8639. [CrossRef] [PubMed]

16. Wang, X.; Wang, Z.M. *Nanoscale Thermoelectrics*; Springer International Publishing: Berlin/Heidelberg, Germany, 2014.

- 17. LaLonde, A.D.; Pei, Y.; Wang, H.; Snyder, G.J. Lead telluride alloy thermoelectrics. *Mater. Today* **2011**, 14, 526–532. [CrossRef]
- 18. Kim, S.I.; Lee, K.H.; Mun, H.A.; Kim, H.S.; Hwang, S.W.; Roh, J.W.; Yang, D.J.; Shin, W.H.; Li, X.S.; Lee, Y.H.; et al. Dense dislocation arrays embedded in grain boundaries for high-performance bulk thermoelectrics. *Science* **2015**, *348*, 109–114. [CrossRef]
- 19. Zhao, L.D.; Lo, S.H.; Zhang, Y.; Sun, H.; Tan, G.; Uher, C.; Wolverton, C.; Dravid, V.P.; Kanatzidis, M.G. Ultralow thermal conductivity and high thermoelectric figure of merit in SnSe crystals. *Nature* **2014**, 508, 373–377. [CrossRef]
- 20. Nozariasbmarz, A.; Zamanipour, Z.; Norouzzadeh, P.; Krasinski, J.S.; Vashaee, D. Enhanced Thermoelectric Performance in Metal/Semiconductor Nanocomposite of Iron Silicide/Silicon Germanium. *RSC Adv.* **2016**, 6, 49643–49650. [CrossRef]
- 21. Nozariasbmarz, A.; Roy, P.; Zamanipour, Z.; Dycus, J.H.; Cabral, M.J.; LeBeau, J.M.; Krasinski, J.S.; Vashaee, D. Comparison of Thermoelectric Properties of Nanostructured Mg<sub>2</sub>Si, FeSi<sub>2</sub>, SiGe, and Nanocomposites of SiGe-Mg<sub>2</sub>Si, SiGe-FeSi<sub>2</sub>. *APL Mater.* **2016**, *4*, 104814. [CrossRef]
- 22. Bell, L.E. Cooling, Heating, Generating Power, and Recovering Waste Heat with Thermoelectric Systems. *Science* **2008**, *321*, 1457–1461. [CrossRef]
- 23. Suarez, F.; Nozariasbmarz, A.; Vashaee, D.; Öztürk, M.C. Designing thermoelectric generators for self-powered wearable electronics. *Energy Environ. Sci.* **2016**, *9*, 2099–2113. [CrossRef]
- 24. Goldsmid, H.J. Recent Studies of Bismuth Telluride and Its Alloys. J. Appl. Phys. 1961, 32, 2198. [CrossRef]
- 25. Wang, S.; Tan, G.; Xie, W.; Zheng, G.; Li, H.; Yang, J.; Tang, X. Enhanced thermoelectric properties of Bi<sub>2</sub>(Te<sub>1-x</sub>Se<sub>x</sub>)<sub>3</sub>-based compounds as n-type legs for low-temperature power generation. *J. Mater. Chem.* **2012**, 22, 20943–20951. [CrossRef]
- 26. Yan, X.; Poudel, B.; Ma, Y.; Liu, W.S.; Joshi, G.; Wang, H.; Lan, Y.C.; Wang, D.Z.; Chen, G.; Ren, Z.F. Experimental studies on anisotropic thermoelectric properties and structures of n-type Bi<sub>2</sub>Te<sub>2.7</sub>Se<sub>0.3</sub>. *Nano Lett.* **2010**, *10*, 3373. [CrossRef]
- Liu, W.S.; Zhang, Q.; Lan, Y.; Chen, S.; Yan, X.; Zhang, Q.; Wang, H.; Wang, D.; Chen, G.; Ren, Z. Thermoelectric Property Studies on Cu-Doped n-type Cu<sub>x</sub>Bi<sub>2</sub>Te<sub>2.7</sub>Se<sub>0.3</sub> Nanocomposites. *Adv. Energy Mater.* 2011, 1, 577–587.
  [CrossRef]
- 28. Hong, M.; Chasapis, T.C.; Chen, Z.G.; Yang, L.; Kanatzidis, M.G.; Snyder, G.J.; Zou, J. n-Type Bi<sub>2</sub>Te<sub>3-x</sub>Se<sub>x</sub> Nanoplates with Enhanced Thermoelectric Efficiency Driven by Wide Frequency Phonon Scatterings and Synergistic Carrier Scatterings. *ACS Nano* **2016**, *10*, 4719–4727. [CrossRef]
- 29. Song, S.; Wang, J.; Xu, B.; Lei, X.; Jiang, H.; Jin, Y.; Zhang, Q.; Ren, Z. Thermoelectric properties of n-type Bi<sub>2</sub>Te<sub>2.7</sub>Se<sub>0.3</sub> with addition of nano-ZnO:Al particles. *Mater. Res. Express* **2014**, *1*, 035901. [CrossRef]
- 30. Hu, L.P.; Liu, X.H.; Xie, H.H.; Shen, J.J.; Zhu, T.J.; Zhao, X.B. Improving thermoelectric properties of n-type bismuth–telluride-based alloys by deformation-induced lattice defects and texture enhancement. *Acta Mater.* **2012**, *60*, 4431–4437. [CrossRef]
- 31. Hu, L.; Zhu, T.; Liu, X.; Zhao, X. Point Defect Engineering of High-Performance Bismuth-Telluride-Based Thermoelectric Materials. *Adv. Funct. Mater.* **2014**, *24*, 5211–5218. [CrossRef]
- 32. Cronin, N.J. Microwave and Optical Waveguides; IOP Publishing: Philadelphia, PA, USA, 1995.
- 33. Nozariasbmarz, A. In-Situ Sintering Decrystallization of Thermoelectric Materials Using Microwave Radiation. Ph.D. Thesis, North Carolina State University, Raleigh, NC, USA, 2017.
- 34. Golio, M. The RF and Microwave Handbook; CRC Press, Taylor and Francis Group: Boca Raton, FL, USA, 2000.
- 35. Oghbaei, M.; Mirzaee, O. Microwave versus conventional sintering: A review of fundamentals, advantages and applications. *J. Alloy. Compd.* **2010**, *494*, 175–189. [CrossRef]
- 36. Thostenson, E.T.; Chou, T.W. Microwave Processing: Fundamentals and Applications. *Compos. Part A* **1999**, 30, 1055–1071. [CrossRef]
- 37. Miller, G.R.; Li, C.Y. Evidence for the existence of antistructure defects in bismuth telluride by density measurements. *J. Phys. Chem. Solids* **1965**, *26*, 173–177. [CrossRef]
- 38. Stterthwaite, C.B.; Ure, R.W., Jr. Electrical and Thermal Properties of Bi<sub>2</sub>Te<sub>3</sub>. *Phys. Rev.* **1957**, *108*, 1164. [CrossRef]

39. Mishra, S.K.; Satpathy, S.; Jepsen, O. Electronic structure and thermoelectric properties of bismuth telluride and bismuth selenide. *J. Phys. Cond. Matter* **1997**, *9*, 461. [CrossRef]

- 40. Horak, J.; Cermak, K.; Koudelka, L. Energy formation of antisite defects in doped Sb<sub>2</sub>Te<sub>3</sub> and Bi<sub>2</sub>Te<sub>3</sub> crystals. *J. Phys. Chem. Solids* **1986**, 47, 805. [CrossRef]
- 41. Pecheur, P.; Toussaint, G. Tight-binding studies of crystal stability and defects in Bi<sub>2</sub>Te<sub>3</sub>. *J. Phys. Chem. Solids* **1994**, *35*, 327. [CrossRef]
- 42. Nozariasbmarz, A.; Hosseini, M.; Vashaee, D. Solid-solution Material Decomposition Induced by Electromagnetic Field: A Non-Equilibrium Thermodynamic Process. 2019; submitted.
- 43. Nozariasbmarz, A.; Dsouza, K.; Vashaee, D. Field Induced Decrystallization of Silicon: Evidence of a Microwave Non-Thermal Effect. *Appl. Phys. Lett.* **2018**, *112*, 093103. [CrossRef]
- 44. Vashaee, D.; Nozariasbmarz, A.; Tayebi, L.; Krasinski, J.S. Microwave processing of thermoelectric materials and use of glass inclusions for improving the mechanical and thermoelectric properties. US Patent App. 15/778, 704, 2018. International Application No.: PCT/US2016/064292.
- 45. Yamashita, O.; Sadatomi, N. Dependence of Seebeck Coefficient on Carrier Concentration in Heavily B- and P Doped  $Si_{1-x}Ge_x$  ( $x \le 0.05$ ) System. *Jpn. J. Appl. Phys.* **1999**, *38*, 6394–6400. [CrossRef]



© 2019 by the authors. Licensee MDPI, Basel, Switzerland. This article is an open access article distributed under the terms and conditions of the Creative Commons Attribution (CC BY) license (http://creativecommons.org/licenses/by/4.0/).